

Active Site Characteristics of CYP4B1 Probed with Aromatic Ligands[†]

Kirk R. Henne, Michael B. Fisher,[‡] Krishna R. Iyer, Dieter H. Lang,[§] William F. Trager, and Allan E. Rettie*

Department of Medicinal Chemistry, School of Pharmacy, University of Washington, Seattle, Washington 98195

Received February 26, 2001; Revised Manuscript Received May 18, 2001

ABSTRACT: The active site topography of rabbit CYP4B1 has been studied relative to CYP2B1 and CYP102 using a variety of aromatic probe substrates. Oxidation of the prochiral substrate cumene by CYP4B1, but not CYP2B1 or CYP102, resulted in the formation of the thermodynamically disfavored ω -hydroxy metabolite, 2-phenyl-1-propanol, with product stereoselectivity for the (*S*)-enantiomer. Reaction of CYP4B1, CYP2B1, and CYP102 with phenyldiazene produced spectroscopically observable σ -complexes for each enzyme. Subsequent oxidation of the CYP2B1 and CYP102 complexes followed by LC/ESI–MS analysis yielded heme pyrrole migration patterns similar to those in previous literature reports. Upon identical treatment, no migration products were detected for CYP4B1. Intramolecular deuterium isotope effects for the benzylic hydroxylation of *o*-xylene- α -²H₃, *p*-xylene- α -²H₃, 2-²H₃,6-dimethylnaphthalene, and 4-²H₃,4'-dimethylbiphenyl were determined for CYP4B1 and CYP2B1 to further map their active site dimensions. These probes permit assessment of the ease of equilibration, within P450 active sites, of oxidizable methyl groups located between 3 and 10 Å apart [Iyer et al. (1997) *Biochemistry* 36, 7136–7143]. Isotope effects for the CYP4B1-mediated benzylic hydroxylation of *o*- and *p*-xylenes were fully expressed (k_H/k_D = 9.7 and 6.8, respectively), whereas deuterium isotope effects for the naphthyl and biphenyl derivatives were both substantially masked (k_H/k_D \approx 1). In contrast, significant suppression of the deuterium isotope effects for CYP2B1 occurred only with the biphenyl substrate. Therefore, rapid equilibration between two methyl groups more than 6 Å apart is impeded within the active site of CYP4B1, whereas for CYP2B1, equilibration is facile for methyl groups distanced by more than 8 Å. Collectively, all data are consistent with the conclusion that the active site of CYP4B1 is considerably restricted relative to CYP2B1.

Cytochrome P450 (CYP)¹ 4B1 is largely an extrahepatic monooxygenase belonging to the P450 superfamily of microsomal heme-containing proteins. Like many mammalian P450s, CYP4B1 does not have a clearly defined endogenous substrate but is known to participate in the metabolism of certain xenobiotic compounds encountered as a result of environmental exposure. Among the known substrates for CYP4B1 are several protoxins, including valproic acid (VPA) (1), 2-aminoanthracene (2, 3), 2-aminoanthracene (2, 4, 5), 3-methylindole (6), and 4-ipomeanol (3, 7). While these compounds have little in common structurally or chemically, their metabolism by CYP4B1 may lead to significant toxicity, thereby rendering CYP4B1 an interesting investigational target.

Rabbit CYP4B1 is an unusually efficient terminal hydroxylase of short–medium-chain fatty acids and the analogous alkane hydrocarbons (8). Such an observation is noteworthy because ω -methyl hydroxylation of hydrocarbon

and fatty acid substrates is energetically less favorable than hydroxylation at methylene carbon atoms (9). Few P450s, other than the CYP4A (10) and CYP4F (11, 12) enzymes, preferentially catalyze ω -methyl hydroxylation, and these latter, more specialized isoforms are thought to act primarily on endobiotic substrates (11, 13, 14) in metabolic pathways engineered by evolutionary design. Given CYP4B1's propensity to bioactivate a variety of rather bulky aromatic xenobiotics, its selective hydroxylation of simple unfunctionalized alkanes at their terminus is quite unusual. The question then arises, what active site topographical features must the CYP4B1 enzyme possess in order to accommodate both ω -specific hydroxylation and tolerance for a wide variety of structurally diverse substrates?

Since detailed three-dimensional structure information is only available for one mammalian P450, CYP2C5 (15), current approaches to elucidating details of the active site structure of the remaining microsomal P450 isoforms are largely indirect. In the present study, we have examined the interaction of cumene, phenyldiazene, and a series of selectively deuterated xylene, dimethylnaphthalene, and dimethylbiphenyl compounds with CYP4B1, CYP102, and

[†] This investigation was supported by Grants GM49054 (A.E.R.) and GM32165 (W.F.T.) from the National Institutes of Health (NIH). K.R.H. was supported by NIH Training Grant GM07750.

* To whom correspondence should be addressed at the Department of Medicinal Chemistry, Box 357610, University of Washington, Seattle, WA 98195. Telephone: (206) 685-0615. Fax: (206) 685-3252. E-mail: rettie@u.washington.edu.

[‡] Present address: Pharmacokinetics, Dynamics, and Metabolism, Pfizer Inc., Eastern Point Road, Groton, CT 06340.

[§] Present address: Drug Metabolism and Isotope Chemistry, Bayer AG, Bldg 466, Wuppertal 42096, Germany.

¹ Abbreviations: CYP, cytochrome P450; HPLC, high-performance liquid chromatography; LC/ESI–MS, liquid chromatography/electrospray ionization–mass spectrometry; GC–MS, gas chromatography–mass spectrometry; FID, flame ionization detector; THF, tetrahydrofuran; DMSO, dimethyl sulfoxide; BSTFA, *N,O*-bis(trimethylsilyl)-trifluoroacetamide; DLPC, L- α -dilauroylphosphatidylcholine.

CYP2B1. Each of these aromatic substrates can provide distinct but complementary information about the characteristics of P450 enzyme active sites.

Aryldiazenes have been used extensively as probes for the active site topography of a variety of P450 isoforms (16), although CYP4B1 has yet to be examined with this approach. Reaction of phenyldiazene with the heme iron results in the formation of an iron–phenyl σ -complex which, upon chemical oxidation, undergoes a rearrangement whereby the phenyl group migrates to one of the four available pyrrole nitrogen atoms. Steric considerations in the active site dictated by the P450 apoprotein direct the shift, and the resulting pattern of *N*-phenylporphyrin regioisomers is used to deduce topographical characteristics.

A new method that has the potential to provide a more quantitative assessment of the spatial limitations within a P450 active site has been developed recently by Iyer et al. (17). Rigid, symmetrical xylenes and a substituted biphenyl (where the distances between methyl groups on the same molecule varied from approximately 3 to 10 Å) were labeled with deuterium on one of the two methyl groups and used to explore the effect of distance on the magnitude of the intrinsic isotope effect for P450-catalyzed benzylic hydroxylation. It was found that the magnitude of the deuterium isotope effect for benzylic hydroxylation of *o*-xylene, *p*-xylene, and 4,4'-dimethylbiphenyl catalyzed by CYP2B1 decreased from a high of near 8 with *o*-xylene to less than 3 with the much larger biphenyl substrate. Therefore, it appears that substrates where motion is not restricted, such that equimolar concentrations of $-\text{CH}_3$ and $-\text{CD}_3$ are presented to the perferryl species of the enzyme, allow full expression of the intrinsic isotope effect. Any barrier to free equilibration of the $-\text{CH}_3$ and $-\text{CD}_3$ groups (as seen with the largest substrate used, 4,4'-dimethylbiphenyl) suppresses this isotope effect. In the present study we have applied this type of analysis to CYP4B1. In addition, we have incorporated a new substrate into the series, 2- $^2\text{H}_3$,6-dimethylnaphthalene, where the distance between oxidizable methyl groups is 8.1 Å, to more fully map the effect of distance on the magnitude of the deuterium isotope effect for P450-catalyzed benzylic hydroxylation.

Finally, since we had established in previous studies (1, 8) that CYP4B1 selectively oxidizes short aliphatic hydrocarbons at their ω -terminus, we also examined the enzyme's metabolic profile toward cumene. This prochiral, aromatic substrate permits an assessment of the enzyme's relative capacity to catalyze ω -hydroxylation versus benzylic hydroxylation, as well as the stereochemistry of formation of any 2-phenyl-1-propanol formed (see Figure 1). Determination of the latter parameter should lend insight into the nature of the enzyme–substrate interaction at the time of catalysis (18).

MATERIALS AND METHODS

Materials. Lithium aluminum deuteride, 2,6-dimethylnaphthalene, 6'-methyl-2'-acetonaphthone, 4-methylbenzyl alcohol, 2-methylbenzyl alcohol, 2,5-dimethylphenol, cumene, (*R*)- and (*S*)-2-phenyl-1-propanol, 2-phenyl-2-propanol, 2-isopropylphenol, 3-isopropylphenol, 4-isopropylphenol, THF, and pyridine were obtained from Aldrich Chemical Co. (Milwaukee, WI). Methyl phenyldiazene carboxylate azo ester

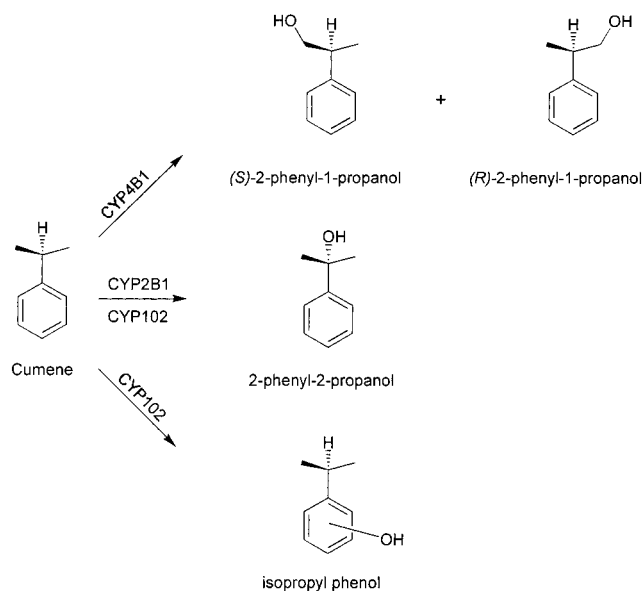


FIGURE 1: Metabolic scheme depicting potential hydroxylated products resulting from the oxidation of cumene by P450 enzymes.

was obtained from Research Organics, Inc. (Cleveland, OH), and bromine and *p*-toluenesulfonyl chloride were from Fluka Chemical Co. (Buchs, Switzerland). Diethyl ether, methylene chloride, and *p*-dioxane were purchased from J. T. Baker, Inc. (Phillipsburg, NJ), pentane was from EM Science (Gibbstown, NJ), and ethyl acetate was from Burdick & Jackson, Inc. (Muskegon, MI). All other organic solvents were from Fisher Scientific (Springfield, NJ). BSTFA was obtained from Supelco, Inc. (Bellefonte, PA), and NADPH and DLPC were from Sigma (St. Louis, MO).

Instrumentation. ^1H NMR of synthetic compounds was carried out using a Varian VXR-300 MHz spectrometer (Varian, Inc., Palo Alto, CA). Data were generated in $\text{DMSO}-d_6$ or CDCl_3 , and chemical shifts reported in parts per million (ppm) relative to internal tetramethylsilane.

GC–FID characterization of cumene metabolites was performed on an HP5890 gas chromatograph interfaced with an HP3396A integrator (Agilent Technologies, Palo Alto, CA). A chiral 30 m Alpha Dex 120 fused silica capillary column was used for analysis (Supelco, Bellefonte, PA). 2-Phenyl-2-propanol, 2-phenyl-1-propanol (partially resolved), 2-isopropylphenol, 4-isopropylphenol, and 3-isopropylphenol eluted at 16.2, 21.8, 26.2, 28.9, and 29.9 min, respectively, with a linear temperature gradient of $2^\circ\text{C}/\text{min}$ from 100°C . Helium was used as a carrier gas at a head pressure of 10 psi. GC–FID characterization of synthetic intermediates and products was performed under similar conditions, with the exception that a 60 m fused silica capillary column coated with a DB-1 stationary phase was used for analyses (J&W Scientific, Folsom, CA).

LC–MS analysis was performed on a Hewlett-Packard LC-MSD Series 1100 quadrupole mass spectrometer (Agilent Technologies, Palo Alto, CA) operating in the electrospray ionization mode. The drying gas temperature was set at 350°C , capillary voltage at 4 kV, and fragmentor voltage at 80 V. The inlet system consisted of a Hewlett-Packard 1100 series binary solvent delivery system, diode array detector, and autosampler. Separation of *N*-phenylporphyrin regioisomers was performed on a self-packed $3\text{ }\mu\text{m}$ C18 reversed-phase HPLC column ($150 \times 2.1\text{ mm}$) at a flow rate of 0.4

mL/min and a mobile phase consisting of 0.1% formic acid, acetonitrile, and isopropyl alcohol (50:40:10).

GC–MS analysis was performed on a Micromass 7070H double focusing mass spectrometer (Micromass Ltd., Manchester, U.K.) interfaced with an HP5890 gas chromatograph containing a 30 m capillary column coated with a DB-5 stationary phase (J&W Scientific, Folsom, CA). The instrument was operated in the electron impact (EI) mode at an electron energy of -70 eV, a trap current of 100 mA, and an accelerating voltage of 4 kV. Ion source and interface temperatures were held at 200 and 250 °C, respectively. During experiments to determine percent deuterium incorporation of synthetic compounds, electron energy was set to -12.5 eV. Data were processed using Windows-based MASPEC software (Mass Spectrometry Services Ltd., Manchester, U.K.).

HPLC separation of 2-phenyl-1-propanol enantiomers was carried out using a Hewlett-Packard 1050 series instrument (Agilent Technologies, Palo Alto, CA) consisting of a quaternary pump, autosampler, and variable wavelength detector. Data generated were analyzed with Windows-based HP1050 ChemStation software. Resolution was achieved on a 150×4.6 mm DAICEL CHIRALPAK AD-RH stationary phase (Chiral Technologies, Inc., Exton, PA) and a hexane/methanol/ethanol mobile phase (97:1.5:1.5). The identity and elution order of (*S*)- and (*R*)-2-phenyl-1-propanol were confirmed using authentic standards available commercially.

Synthesis of o-Xylene- α - $^2\text{H}_3$, p-Xylene- α - $^2\text{H}_3$, and 4- $^2\text{H}_3$,4'-Dimethylbiphenyl. The selectively deuterated xylenes and 4,4'-dimethylbiphenyl were synthesized as described previously (17).

Synthesis of 2- $^2\text{H}_3$,6-Dimethylnaphthalene. Bromine (1.7 mL, 33 mmol) was added to a stirred 5 M solution of NaOH (20 mL) in an ice bath. After 10 min, 6'-methyl-2'-acetophenone (2 g, 10.9 mmol) suspended in dioxane (10 mL) was added dropwise over a 15 min period. The reaction was allowed to proceed for 2.5 h before the addition of water (5 mL) and 0.35 M sodium metabisulfite (5 mL). Concentrated HCl was then used to acidify the mixture, which was cooled in an ice bath for 20 min prior to filtration. The resulting product, 6-methyl-2-naphthoic acid, was recrystallized first from ethyl acetate and then from chloroform. In the subsequent step, lithium aluminum deuteride (2 g, 16.2 mmol) was dissolved in dry THF (30 mL) and allowed to stir on ice before the dropwise addition of 6-methyl-2-naphthoic acid (0.75 g, 4.1 mmol) in THF (20 mL). After 4 h, the reaction was quenched with ice-cold water, acidified with concentrated HCl, and extracted with 2×100 mL of diethyl ether. The extracts were combined and dried over magnesium sulfate, and the solvent was removed under reduced pressure to yield the crude alcohol- d_2 product (800 mg). Subsequent tosylation was initiated by first dissolving the alcohol- d_2 (410 mg, 2.5 mmol) in methylene chloride (15 mL) and pyridine (1 mL). The solution was then stirred in an ice bath prior to the addition of *p*-toluenesulfonyl chloride (579 mg, 3.0 mmol) suspended in methylene chloride (2 mL). The reaction was warmed to ambient temperature and allowed to react overnight. Next, the solvent was removed under reduced pressure, and the crude tosylated product was redissolved in dry THF (20 mL) before its dropwise addition to a stirred suspension of lithium aluminum deuteride (0.5 g) in THF (30 mL). After 3 h, the

reduction was quenched with ice-cold water, acidified with concentrated HCl, and extracted with 3×50 mL of diethyl ether. Extracts were combined and dried over magnesium sulfate, and the solvent was removed under reduced pressure. Crude 2- $^2\text{H}_3$,6-dimethylnaphthalene was purified over silica using hexane as the eluent. The resulting product (41 mg, 0.26 mmol) was $>99\%$ pure by GC and by GC–MS had a deuterium content of 98.26 atom % deuterium- d_3 , 1.60 atom % deuterium- d_2 , and 0.14 atom % deuterium- d_1 . ^1H NMR (CHCl_3): δ 2.50 (s, 3H, Ar- CH_3), 7.29 (d, $J = 9.3$ Hz, 2H, Ar-H), 7.57 (s, 2H, Ar-H), 7.67 (d, $J = 8.3$ Hz, 2H, Ar-H).

Purified P450s and Coenzymes. CYP2B1 was purified from phenobarbital-pretreated Sprague–Dawley rats as described (19), and CYP102 was induced in *Bacillus megaterium* with pentobarbital prior to purification according to the method of Black et al. (20), with minor modifications. Baculovirus expression and purification of rabbit CYP4B1 were also performed according to a published procedure (21). Recombinant rat NADPH-P450 oxidoreductase and human cytochrome b_5 were expressed and purified from bacterial cultures in a manner described previously by Chen et al. (22).

Formation of the Iron–Phenyl σ -Complex, Migration, and Analysis of the Resulting N-Phenylporphyrin Regioisomers. To a quartz cuvette was added each CYP (0.5–5 nmol) in either 1 mL of 100 mM potassium phosphate buffer (pH 7.4) or 1 mL of 50 mM potassium phosphate buffer containing 20% glycerol and 0.1 mM EDTA (pH 7.4). Phenyl diazene was generated fresh for each experiment by mixing 2.5 μL of methyl phenyldiazene carboxylate azo ester with 200 μL of 1 M NaOH. An aliquot of the resulting solution (1 μL) was added to the contents of the cuvette, and absorbance was measured from 350 to 650 nm. Iron–phenyl complex formation was determined by peak formation around 480 nm. After peak formation at 480 had reached a maximum, the reaction was allowed to continue for an additional 15 min. Potassium ferricyanide (1 μL of a 50 mM solution) was then added, and loss of the 480 nm peak was monitored spectroscopically. After 15 min, the cuvette contents were diluted with 5% aqueous H_2SO_4 (5 mL) and allowed to stand for 2–4 h at 4 °C. The solution was extracted with CH_2Cl_2 (2×5 mL), the combined organic layers were evaporated, and the residue was reconstituted in 200 μL of an HPLC mobile phase consisting of 0.1% formic acid, acetonitrile, and isopropyl alcohol (50:40:10). Detection was by LC/ESI–MS, and analysis was by selected ion monitoring of the $[\text{M} + \text{H}]^+$ ion for each *N*-phenylporphyrin isomer at m/z 639. A mixture of standards for each of the four *N*-phenylporphyrin IX regioisomers (N_A , N_B , N_C , and N_D) was generated from myoglobin as reported in the literature (23).

Intramolecular Deuterium Isotope Effect Determination for the Benzylic Hydroxylation of o-Xylene- α - $^2\text{H}_3$, p-Xylene- α - $^2\text{H}_3$, 2- $^2\text{H}_3$,6-Dimethylnaphthalene, and 4- $^2\text{H}_3$,4'-Dimethylbiphenyl. CYP4B1 or CYP2B1 (50–500 pmol) was reconstituted with P450 reductase (100–500 pmol), L- α -dilauroylphosphatidylcholine (DLPC) (10–20 μg), and cytochrome b_5 (50 pmol, CYP4B1 only) in 100 mM potassium phosphate buffer (pH 7.4) to a total volume of 1 mL. CYP102 (0.5–1.0 nmol) was solubilized in 100 mM potassium phosphate buffer (pH 7.4) only. Each deuterated substrate was then added to a final concentration of 1 mM.

Reactions were initiated by the addition of NADPH (1 mM final concentration) and allowed to proceed at 37 °C for 30 or 45 min. After this time, reactions were immediately extracted with ice-cold pentane (2 × 3 mL), dried with magnesium sulfate, and evaporated to approximately 30 μ L under a stream of dry N₂. Derivatization was then carried out at 70 °C for 30 min by the addition of 100 μ L of a 1:1 mixture of BSTFA and ethyl acetate. Analysis was performed by GC–MS in the selected ion monitoring (SIM) mode. Ions monitored corresponded to the [M – 15]⁺ fragments generated from the trimethylsilylated hydroxy metabolites of the selectively deuterated xylenes, naphthyl, and biphenyl compounds. The xylenes were injected on the column at an oven temperature of 80 °C, held at constant temperature for 1 min, and eluted with a linear temperature gradient of 5 °C/min to 140 °C. Similarly, the naphthyl and biphenyl metabolites were injected on the column at an oven temperature of 130 °C, held at constant temperature for 1 min, and eluted with a linear temperature gradient of 10 °C/min to 270 °C. The retention times of all metabolites were confirmed by comparison to retention times of synthetic standards or those commercially available. Helium was used as the carrier gas at a head pressure of 10 psi. Isotope effect values were calculated using the peak areas of the appropriate ions, and corrections were made as previously described for natural isotopic abundance and incomplete deuterium incorporation into the substrates (17).

Metabolism of Cumene by CYP Enzymes. CYP4B1 or CYP2B1 (100 pmol) was reconstituted with P450 reductase (200 pmol), DLPC (10 mg), and cytochrome *b*₅ (100 pmol, CYP4B1 only) in 100 mM potassium phosphate buffer (pH 7.4) to a total volume of 1 mL. CYP102 (500 pmol) was solubilized in 100 mM potassium phosphate buffer only (pH 7.4). Cumene was added to a final concentration of 100 μ M, and reactions were initiated by the addition of NADPH (1 mM final concentration) and allowed to proceed at 37 °C for 30 min. After this time, reactions were immediately extracted with ice-cold pentane (2 × 3 mL), dried with magnesium sulfate, and evaporated to approximately 30 μ L under a stream of dry N₂. Extracts were brought to a final volume of 100 μ L in the HPLC mobile phase, consisting of hexane/methanol/ethanol (97:1.5:1.5), before injection onto the chiral column.

Other Methods. P450 measurements were taken using the method of Estabrook et al. (24). Kinetic evaluation of cumene metabolism by CYP4B1 was performed over a substrate concentration range of 5–1000 μ M. *K*_m and *V*_{max} were determined using the *k*.cat software package (v1.5, BioMetallics, Inc., Princeton, NJ).

RESULTS

Regioselective Metabolism of Cumene by CYP4B1 and Determination of the 2-Phenyl-1-propanol (*S*)/(*R*) Ratio. CYP4B1, CYP2B1, and CYP102 each metabolized cumene to hydroxylated products (Figure 1) although turnover with CYP102 was low relative to the other two enzymes. Both CYP102 and CYP2B1 preferentially formed the benzylic metabolite, 2-phenyl-2-propanol, whereas CYP4B1 metabolized cumene almost exclusively at the ω -methyl group, yielding an ω : ω – 1 ratio of >27:1 (Table 1). Only CYP102 formed significant phenol, and none of the enzyme prepara-

Table 1: Summary of Cumene Metabolism by Selected CYP Enzymes

P450 enzyme	$\omega/(\omega - 1)$	(<i>S</i>):(<i>R</i>) 2-phenyl-1-propanol
CYP4B1 ^a	>27	2.9:1
CYP102	<0.2	
CYP2B1	<0.01	

^a Turnover of cumene to 2-phenyl-1-propanol by CYP4B1 exhibited a *K*_m of 105 μ M and a *V*_{max} of 18 nmol/min.

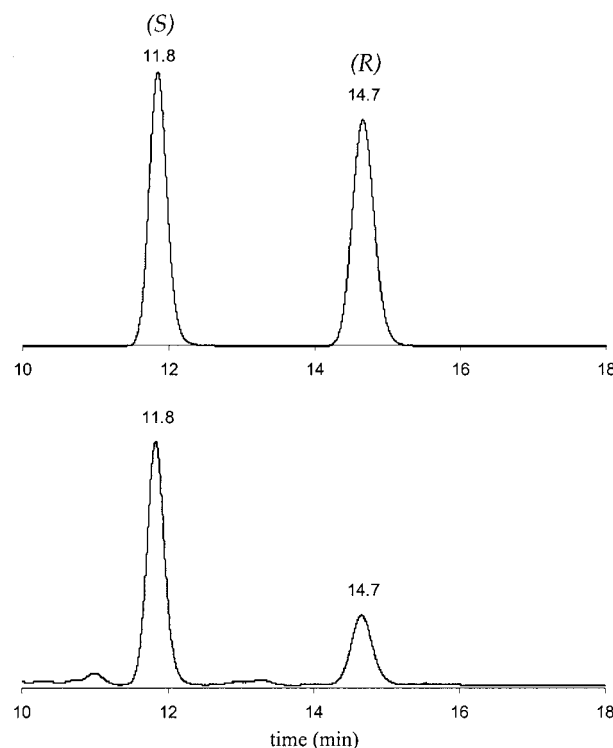


FIGURE 2: Upper panel: LC–UV chromatogram showing the resolution of racemic 2-phenyl-1-propanol standard. Peak labels indicate retention time and the stereochemical identity of each chiral compound. Lower panel: LC–UV chromatogram of a pentane extract from a CYP4B1 incubation with cumene. On the basis of integrated peak areas, the ratio of (*S*)-2-phenyl-1-propanol to (*R*)-2-phenyl-1-propanol is 2.9:1.

tions yielded α -methylstyrene as a significant metabolite. The (*S*)- and (*R*)-enantiomers of 2-phenyl-1-propanol could be separated by chiral-phase HPLC with baseline resolution, as shown in Figure 2. Analysis of the chiral metabolites generated by CYP4B1 gave an (*S*)/(*R*) ratio of 2.92:1 \pm 0.004 (mean \pm SD, *n* = 4). Therefore, to a notable degree, the active site environment of CYP4B1 not only can overcome thermodynamically preferred benzylic hydroxylation in favor of ω -hydroxylation of cumene but also can distinguish between the substrate's two chemically equivalent methyl groups.

Iron–Phenyl Complex Formation, Migration, and Analysis of *N*-Phenylporphyrin Adducts. CYP4B1, CYP102, and CYP2B1 each displayed a characteristic spectroscopic signature at 480 nm upon treatment with phenyldiazene, indicating formation of an iron–phenyl complex (Figure 3). Subsequent oxidation of the complex by the addition of potassium ferricyanide resulted in the immediate loss of the 480 nm absorbance in each case. We confirmed by HPLC that mild acid treatment released heme from all three

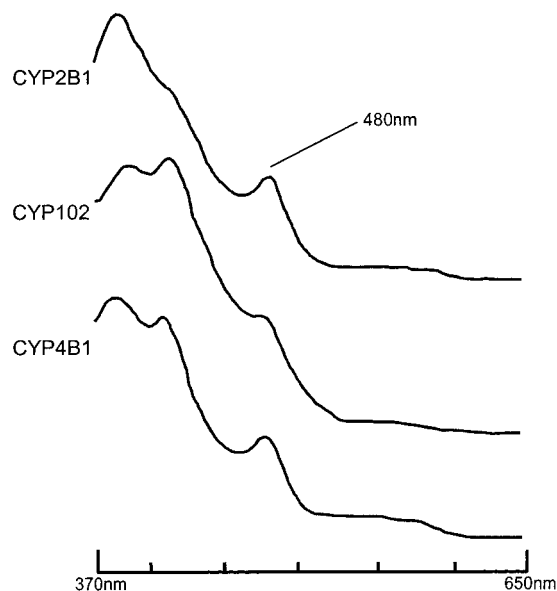


FIGURE 3: UV absorption spectra demonstrating formation of iron–phenyl complexes at 480 nm following reaction of phenyldiazene with CYP2B1, CYP102, and CYP4B1.

enzymes examined in the present study (data not shown). However, the yield of heme obtained from acidified samples of CYP4B1 was relatively low compared to CYP2B1 and CYP102, so we developed a sensitive LC–MS procedure that could detect as little as 1 ng of *N*-phenylporphyrin. LC–MS analysis of extracted *N*-phenylporphyrins gave expected ratios of the four regioisomers in the case of both CYP2B1 and CYP102 (Figure 4). An $N_B:N_A:N_C:N_D$ isomeric ratio of 2:32:8:58 was obtained for CYP2B1, which agreed well with a previously reported determination where N_A and N_D adducts were shown to predominate (25). Results from experiments performed with CYP102 gave a ratio of 8:72:12:8, where the major product is the N_A isomer. This finding was also quite similar to that published previously (16) and may be taken as an indication of a more congested active site environment for CYP102 than is present in CYP2B1. However, despite exhaustive attempts to determine an isomeric ratio of phenyl migration products in experiments that used up to 5 nmol of CYP4B1, oxidation of the spectral iron–phenyl complex did not yield detectable quantities of *N*-phenylporphyrins—even with sensitive MS detection (Figure 4). The small broad peak present in the CYP4B1 LC–MS trace at about 27 min is a component of the enzyme preparation also seen in untreated samples. This peak did not exhibit a UV absorbance at 400 nm (data not shown) and, therefore, does not represent formation of either the N_C or N_D isomers. These data imply a highly congested active site in CYP4B1.

Intramolecular Deuterium Isotope Effects for Benzylic Hydroxylation of Selectively Deuterated Xylene, Naphthyl, and Biphenyl Substrates by CYP4B1, CYP2B1, and CYP102. Comparison of the deuterium isotope effect profiles for a series of rigid, aromatic substrates where the distance between labeled and unlabeled methyl groups varies is expected to provide useful information on relative active site dimensions for different cytochrome P450 isoforms. Accordingly, we synthesized deuterated 2- $^2\text{H}_3$,6-dimethylnaphthalene, an additional member of the original series (see Table 2), and determined the isotope effect profiles for the

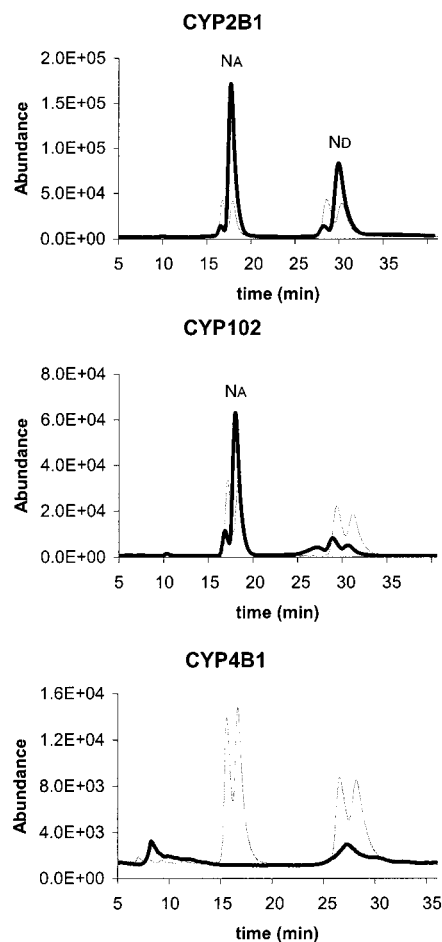


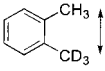
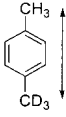
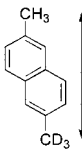
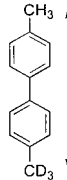
FIGURE 4: LC/ESI–MS chromatograms of enzyme-derived *N*-phenylporphyrins at m/z 639.5. The darker traces represent *N*-phenylporphyrins extracted from P450, whereas the lighter traces represent *N*-phenylporphyrin standards derived from myoglobin. The elution order of the *N*-phenylporphyrin regioisomers is $N_B:N_A:N_C:N_D$.

fatty acid hydroxylases, CYP4B1 and CYP102, as well as for CYP2B1. The corrected intramolecular deuterium isotope effects for *o*-xylene- α - $^2\text{H}_3$, *p*-xylene- α - $^2\text{H}_3$, 2- $^2\text{H}_3$,6-dimethylnaphthalene, and 4- $^2\text{H}_3$,4'-dimethylbiphenyl are summarized in Table 3. The range of values obtained for CYP2B1, from 8.82 down to 3.23 for the xylene and biphenyl substrates, is similar to that obtained previously (17). As expected, the isotope effect of 6.48 obtained for the dimethylnaphthalene substrate is intermediate between that obtained with *p*-xylene and 4,4'-dimethylbiphenyl. However, the isotope effect profile for the same set of deuterated compounds and CYP4B1 is markedly different. Isotope effects for the naphthyl and biphenyl substrates are completely suppressed (0.92 ± 0.01 and 1.07 ± 0.01 , respectively), while both *o*-xylene and *p*-xylene exhibit values close to those obtained with CYP2B1. These data indicate that the active site of CYP4B1 is considerably more restricted than it is in CYP2B1. Efforts to characterize CYP102 using the selectively deuterated aromatic substrates were impeded by extremely low turnover to the benzylic metabolites.

DISCUSSION

In the present study we have attempted to gain insight into the active site environment of CYP4B1 by analyzing

Table 2: Selectively Deuterated Substrates Used for Intramolecular Isotope Effect Studies

	 o-xylene-α- ² H ₃	 p-xylene-α- ² H ₃	 2- ² H ₃ ,6-dimethyl- naphthalene	 4- ² H ₃ ,4'-dimethyl- biphenyl
methyl group distance ^a (Å)	3.0	5.9	8.1	10.3
area (Å ²)	7.0	27	51	84

^a Distances were determined on energy-minimized structures using Spartan software (v4.04, Wavefunction, Inc., Irvine, CA). ^b Circular areas required for methyl group equilibration were calculated assuming a radius equal to half the methyl group distance.

Table 3: Intramolecular Deuterium Isotope Effects on the Benzylic Hydroxylation of Selectively Deuterated Substrates for CYP2B1, CYP102, and CYP4B1^a

deuterated substrate	CYP enzyme		
	CYP2B1	CYP102	CYP4B1
o-xylene	8.82 (0.05)	ND	9.72 (0.02)
p-xylene	6.96 (0.05)	ND	6.81 (0.03)
2,6-dimethylnaphthalene	6.48 (0.08)	ND	0.92 (0.01)
4,4'-dimethylbiphenyl	3.23 (0.06)	ND	1.07 (0.01)

^a Numbers in parentheses reflect standard deviations for at least three determinations. ND = no data; turnover of these substrates was too low for the accurate determination of isotope effect values.

the interactions of the enzyme with several aromatic substrates. The pronounced tendency of CYP4B1 to hydroxylate the terminal carbon atom of aliphatic hydrocarbons (8) prompted us to determine the regiochemistry and stereochemistry of cumene metabolites generated by the purified enzyme. Previous reports have documented selective ω -1 hydroxylation of cumene and modest stereochemical preferences for formation of the minor ω -hydroxy metabolite in studies conducted with rat liver microsomes (18) and in vivo in rabbits (26). Recombinant rabbit CYP4B1 exhibited pronounced regioselectivity for ω -hydroxylation of cumene and a significant prochiral selectivity for formation of the (S)-2-phenyl-1-propanol metabolite. This indicates that active site constraints in the immediate vicinity of the CYP4B1 perferryl species must play some role in orienting the *pro*-(S) methyl group of cumene for catalysis. However, application of the Arrhenius equation (27) equates the enantiomeric ratio of 2.9:1 observed for methyl group hydroxylation to a differential energy barrier of only 0.7 kcal/mol. Therefore, this interaction does not appear to be as significant as those necessary to ensure selective ω -hydroxylation of cumene, where bond dissociation energies for removal of hydrogen from a benzylic site (\sim 85 kcal/mol) and an aliphatic ω -methyl carbon (\sim 98 kcal/mol) (9) differ by more than 10 kcal/mol.

Aryldiazene form aryl-iron complexes with many P450s. These complexes rearrange upon oxidation to stable *N*-arylporphyrins, the regioisomeric distribution of which is believed to reflect the unhindered space above the plane of the heme prosthetic group (16). This technique has been validated by comparing the open volumes inferred from rearrangement studies with crystallographic data obtained for several of the soluble P450s (28–30). Not all P450 enzymes, however, are amenable to this approach. Previous attempts

to use phenyldiazene to examine the active site environment of the closely related CYP4A1 enzyme failed even to give evidence of an iron-phenyl σ -complex intermediate (31). In this instance, the authors concluded that the steric constraints of the active site of CYP4A1 prohibited formation of the complex. In the case of CYP4B1, a σ -complex can be formed, but we were not able to induce migration of the phenyl group by treatment with ferricyanide. Because both CYP4A1 and CYP4B1 function as ω -hydroxylases, it seems likely that the active site steric restrictions that are responsible for orienting substrates in a position suitable for oxidation at the ω -terminus also prevent formation of *N*-phenylporphyrin adducts in both enzymes.

The determination of intramolecular deuterium isotope effect profiles for the P450-catalyzed benzylic hydroxylation of a series of selectively deuterated xylene and dimethylbiphenyl substrates is an emerging technique aimed at obtaining a more quantitative assessment of steric restrictions in a P450 active site (17). Metabolism of a symmetrical compound having two possible oxidation sites that differ only by the presence of hydrogen at one site and deuterium at the other will give rise to an intrinsic isotope effect (k_H/k_D) if the compound has unrestricted movement in the active site at the time of oxidation. Conversely, a more confined active site should slow the equilibration rate of the isotopically distinct oxidation sites, thereby suppressing the isotope effect. The methyl group distance that results in complete suppression of the isotope effect should be reflective of the P450 active site dimensions. In the present study, we obtained a value of 6.5 for the deuterium isotope effect on CYP2B1-mediated benzylic hydroxylation of a new member of the series, 2-²H₃,6-dimethylnaphthalene. This value falls between that determined for *p*-xylene (7.0) and dimethylbiphenyl (3.2). Because the distance between the methyl groups in this substrate (8.1 Å) is also intermediate between the methyl group distances in *p*-xylene and 4,4'-dimethylbiphenyl (5.9 and 10.3 Å, respectively), the isotope effect–distance association reported previously for CYP2B1 (17) is confirmed.

In the earlier work by Iyer et al. (17), bis(monodeuteriomethyl) (*d*₂) and bis(dideuteriomethyl) (*d*₄) analogues of each of the xylene and 4,4'-dimethylbiphenyl substrates were used to determine the intrinsic isotope effect (k_H/k_D) on benzylic oxidation in the absence of a notable distance separating protio and deuterio sites. For these six substrates, only facile bond rotation would be required for equilibration, and the observed isotope effect, (k_H/k_D)_{obs}, should approximate the

intrinsic value after statistical correction. The d_2 and d_4 substrates, therefore, established a standard against which isotope effects generated by the d_3 substrates could be compared in order to fairly evaluate isotope effect suppression resulting from the distance between labeled sites. The results from these experiments clearly demonstrated that not only are the *intrinsic* isotope effects similar across the series of substrates for different P450s (6.09 ± 0.87 , $n = 24$) but the calculated primary isotope effects (P) are as well (6.20 ± 0.72 , $n = 24$). Iyer et al. concluded that “reasonably constant values of P over all the substrates and enzyme preparations provide further support for the notion that the intrinsic isotope effect for a given oxidative reaction is likely to be substantially independent of the specific P450 catalyzing the reaction”. In light of this finding, the intrinsic isotope effect and primary isotope effect for benzylic oxidation of dimethylnaphthalene are expected to be the same as the xylene and dimethylbiphenyl substrates regardless of which P450 is catalyzing the oxidation. As such, in the present study, d_2 and d_4 analogues of the new dimethylnaphthyl probe were not examined. The isotope effects observed with the dimethylnaphthalene substrate are assumed to be fully expressed if the value is greater than 6.5, in accordance with the related substrates in the previous work.

Interestingly, the mechanism by which cytochrome P450 catalyzes aliphatic hydroxylation is currently a matter of some debate. The long-held view has been that the reaction proceeds via a stepwise radical mechanism involving initial abstraction of a hydrogen atom by the perferryl bound oxygen atom of the enzyme. Indeed, the large deuterium isotope effects generally associated with aliphatic hydroxylation have constituted one of the primary lines of evidence in support of this mechanism (32). However, within the past few years, several studies by Newcomb et al. have challenged this view (33–35). The results of their analysis of P450-mediated metabolism of “hypersensitive radical clocks” require that, for some substrates, hydroxy radical rebound must occur at an impossibly fast rate if a two-step radical mechanism is to govern the reaction. Consequently, an alternative mechanism has evolved that features asynchronous oxygen insertion across the carbon–hydrogen bond. Most recently, Shaik and co-workers (36, 37) have studied aliphatic hydroxylation using high-level theoretical calculations, and a two-state reactivity model for P450 hydroxylation has emerged that appears to resolve the seemingly contradictory evidence supporting either the two-step radical mechanism or the asynchronous insertion mechanism. In any event, it is important to note that the *changes* in the magnitude of the deuterium isotope effects used in this paper as an indicator of active site space are independent of the mechanism of hydroxylation. Thus, whatever the mechanism, if the measured deuterium isotope effect is as large as the intrinsic isotope effect for that oxidative reaction, the rate of equilibration of equivalent protio and deuterio sites on the molecule must be fast relative to bond breaking. Conversely, any decrease in the magnitude of the deuterium isotope effect must reflect an imbalance in the relative concentrations of protio and deuterio sites seen by the active oxygen as a result of the rate of equilibration being similar to or less than the rate of bond breaking.

While it is generally believed that equilibration between deuterio and protio sites on the same carbon atom is governed

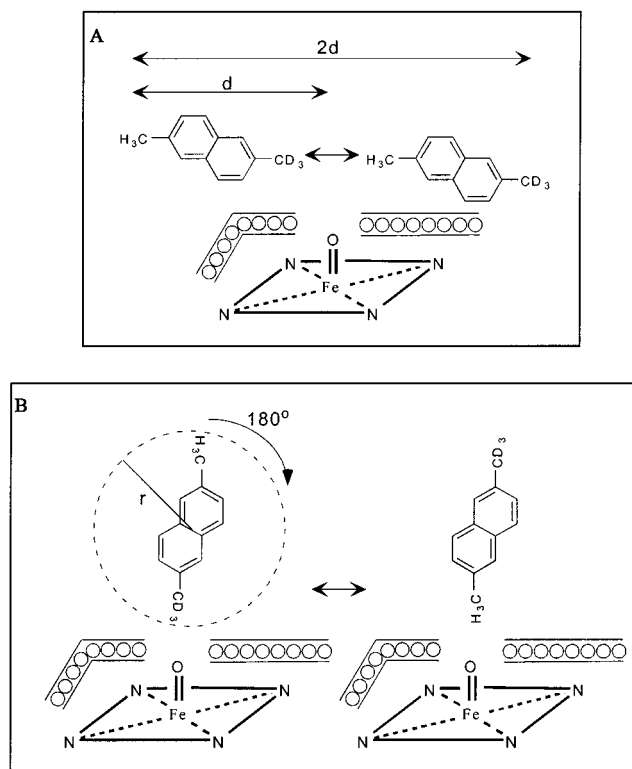


FIGURE 5: Schematic diagram depicting the equilibration of 2,2- $\text{H}_3,6$ -dimethylnaphthalene in the CYP4B1 active site via translational motion (panel A) and rotational motion (panel B). The active site “length” must be at least twice the distance (d) separating the methyl groups in order to accommodate translational equilibration. Rotational equilibration may also occur about the C_2 symmetry axis describing a circular area of radius r , equal to $d/2$. In both panels, the connected circles depict protein amino acid residues restricting substrate access above the heme nitrogen atoms, as suggested by phenyldiazene experiments.

by a single bond rotation (as with the d_2 and d_4 compounds), the mode of equilibration for the d_3 substrates is necessarily more complex. A recent computational study that modeled the motion of xylenes in the active site of CYP101 (P450_{CAM}) suggested that movement of these substrates is predominantly of a translational nature (38). In the most simple case, a substrate experiencing facile equilibration between isotopically sensitive sites must translate a distance equal to that separating the two methyl groups in a length of space twice the distance between them (assuming one-dimensional movement) (Figure 5A). If we apply this consideration to the P450 enzymes studied here, the distance between methyl groups of the largest substrate exhibiting an unsuppressed isotope effect will reflect approximately half the maximal distance across the active site of the enzyme. For CYP2B1, metabolism of deuterated 2,6-dimethylnaphthalene gives rise to a relatively high, although partially suppressed isotope effect, whereas substantial suppression can be seen with deuterated 4,4'-dimethylbiphenyl. If indeed the naphthyl substrate undergoes relatively little translational impedance, its methyl group distance of 8.1 Å would correspond to an active site width of 16.2 Å. Extension of this argument to CYP4B1, where the largest substrate allowed facile equilibration is *p*-xylene- α - $^2\text{H}_3$ (5.9 Å between methyl groups), suggests that the CYP4B1 active site width (11.8 Å calculated by this method) is smaller than that of CYP2B1 by at least 4 Å.

However, our data demonstrating a lack of phenyldiazene rearrangement products from CYP4B1, the enzyme's high degree of ω -selectivity for alkane hydroxylation, and the absence of CYP4B1-derived phenolic metabolites from the deuterated probes all suggest that translational motion of these substrates near the active oxygen species of CYP4B1 is not favored. Therefore, it seems more likely that restricted equilibration of the methyl groups of 2-²H₃,6-dimethylnaphthalene implied by the low deuterium isotope effect for this probe is a consequence of impeded end-on rotational motion of the substrate as shown in Figure 5B. If rotational equilibration is favored over translation motion, the active site dimensions of CYP4B1 and CYP2B1 may be compared in terms of two-dimensional areas (Figure 5B). Given that rotation about the C₂ symmetry axis (for *p*-xylene, 2,6-dimethylnaphthalene, and 4,4'-dimethylbiphenyl) would approximate the least space required for methyl group equilibration, circular areas can be calculated assuming a radius half the distance between the methyl groups. Using the radii of the naphthyl and *p*-xylene substrates, we estimate CYP2B1's active site area to be at least 50 Å², while the area estimation for CYP4B1 is less than 30 Å². These calculations, in terms of either active site width or area, suggest that a relatively restricted active site region in CYP4B1 is likely to be responsible for the selective terminal hydroxylation of aliphatic hydrocarbon substrates.

Interestingly, 2-²H₃,6-dimethylnaphthalene shares structural similarities to the known procarcinogen, 2-aminonaphthalene, which has been shown to be bioactivated by rat CYP4B1 in the *umu* gene expression assay (39). Given their structural similarities, 2-aminonaphthalene and 2,6-dimethylnaphthalene may bind well to CYP4B1 orthologues whose restricted active sites dictate the end-on orientation shown in Figure 5B. Since no aromatic oxidation products were observed from CYP4B1-mediated metabolism of 2-²H₃,6-dimethylnaphthalene, active site constraints of the enzyme alluded to above may render CYP4B1 capable only of bioactivating 2-aminonaphthalene through oxidation at the amino substituent by disfavoring binding conformations that would generate potentially less toxic phenolic products.

One of the objectives of the present work was to compare isotope effect data generated from CYP4B1 to that obtained with an enzyme of related function, CYP102, for which several crystal structures are available (40–44). However, benzylic hydroxylation was a very minor pathway for metabolism of the deuterated xylenes, and so this aim could not be accomplished with the native enzyme. We reasoned that this was probably due to the sequestration of the benzylic methyl group in a pocket dictated by the presence of the phenylalanine residue at position 87, as indicated in the crystal structure of the enzyme with palmitoleic acid bound at the active site (40). In support of this we have found in preliminary experiments that the CYP102 F87G mutant carries out benzylic hydroxylation with relative ease (data not shown).

In summary, cumene metabolite profiles, phenyldiazene migration experiments, and intramolecular deuterium isotope effect profiles are all consistent with a restricted CYP4B1 active site. Selective ω -hydroxylation and the lack of identifiable phenyldiazene migration adducts to the heme are characteristics common to both CYP4B1 and CYP4A1. The active site topography of the CYP4A subfamily has been

studied extensively by many investigators employing a wide range of techniques (31, 45, 46). From the results of the present studies and the consensus view on CYP4A1, it seems likely that both enzymes possess a restricted active site channel, at least in the immediate vicinity of their heme prosthetic groups. However, since CYP4B1 displays a wider substrate specificity than CYP4A1 and is not reliant on polar or electrostatic enzyme–ligand interactions to accomplish selective ω -hydroxylation (8), substantial differences must exist between the two enzymes at more distal sites within the binding pocket.

REFERENCES

1. Rettie, A. E., Sheffels, P. R., Korzekwa, K. R., Gonzalez, F. J., Philpot, R. M., and Baillie, T. A. (1995) *Biochemistry* 34, 7889–7895.
2. Robertson, I. G., Serabjit-Singh, C., Croft, J. E., and Philpot, R. M. (1983) *Mol. Pharmacol.* 24, 156–162.
3. Smith, P. B., Tiano, H. F., Nesnow, S., Boyd, M. R., Philpot, R. M., and Langenbach, R. (1995) *Biochem. Pharmacol.* 50, 1567–1575.
4. Vanderslice, R. R., Boyd, J. A., Eling, T. E., and Philpot, R. M. (1985) *Cancer Res.* 45, 5851–5858.
5. Robertson, I. G. (1986) *Mutat. Res.* 175, 153–157.
6. Thornton-Manning, J., Appleton, M. L., Gonzalez, F. J., and Yost, G. S. (1996) *J. Pharmacol. Exp. Ther.* 276, 21–29.
7. Verschoyle, R. D., Philpot, R. M., Wolf, C. R., and Dinsdale, D. (1993) *Toxicol. Appl. Pharmacol.* 123, 193–198.
8. Fisher, M. B., Zheng, Y. M., and Rettie, A. E. (1998) *Biochem. Biophys. Res. Commun.* 248, 352–355.
9. Kerr, J. A. (1966) *Chem. Rev.* 66, 465–500.
10. Roman, L. J., Palmer, C. N., Clark, J. E., Muerhoff, A. S., Griffin, K. J., Johnson, E. F., and Masters, B. S. (1993) *Arch. Biochem. Biophys.* 307, 57–65.
11. Jin, R., Koop, D. R., Raucy, J. L., and Lasker, J. M. (1998) *Arch. Biochem. Biophys.* 359, 89–98.
12. Kikuta, Y., Kusunose, E., Kondo, T., Yamamoto, S., Kinoshita, H., and Kusunose, M. (1994) *FEBS Lett.* 348, 70–74.
13. Rendic, S., and Di Carlo, F. J. (1997) *Drug Metab. Rev.* 29, 413–580.
14. Makita, K., Falck, J. R., and Capdevila, J. H. (1996) *FASEB J.* 10, 1456–1463.
15. Williams, P. A., Cosme, J., Sridhar, V., Johnson, E. F., and McRee, D. E. (2000) *Mol. Cell.* 5, 121–131.
16. Ortiz de Montellano, P. R. (1995) *Biochimie* 77, 581–593.
17. Iyer, K. R., Jones, J. P., Darbyshire, J. F., and Trager, W. F. (1997) *Biochemistry* 36, 7136–7143.
18. Sugiyama, K., and Trager, W. F. (1986) *Biochemistry* 25, 7336–7343.
19. Rettie, A. E., Rettenmeier, A. W., Howald, W. N., and Baillie, T. A. (1987) *Science* 235, 890–893.
20. Black, S. D., Linger, M. H., Freck, L. C., Kazemi, S., and Galbraith, J. A. (1994) *Arch. Biochem. Biophys.* 310, 126–133.
21. Guan, X., Fisher, M. B., Lang, D. H., Zheng, Y. M., Koop, D. R., and Rettie, A. E. (1998) *Chem. Biol. Interact.* 110, 103–121.
22. Chen, W., Koenigs, L. L., Thompson, S. J., Peter, R. M., Rettie, A. E., Trager, W. F., and Nelson, S. D. (1998) *Chem. Res. Toxicol.* 11, 295–301.
23. Swanson, B. A., and Ortiz de Montellano, P. R. (1991) *J. Am. Chem. Soc.* 113, 8146–8153.
24. Estabrook, R. W., Baron, J., Peterson, J., and Ishimura, Y. (1972) *Biochem. Soc. Symp.* 34, 159–185.
25. Tuck, S. F., and Ortiz de Montellano, P. R. (1992) *Biochemistry* 31, 6911–6916.
26. Ishida, T., and Matsumoto, T. (1992) *Xenobiotica* 22, 1291–1298.
27. Light, D. R., Waxman, D. J., and Walsh, C. (1982) *Biochemistry* 21, 2490–8.

28. Tuck, S. F., Peterson, J. A., and Ortiz de Montellano, P. R. (1992) *J. Biol. Chem.* 267, 5614–5620.
29. Raag, R., Swanson, B. A., Poulos, T. L., and Ortiz de Montellano, P. R. (1990) *Biochemistry* 29, 8119–8126.
30. Fruetel, J. A., Mackman, R. L., Peterson, J. A., and Ortiz de Montellano, P. R. (1994) *J. Biol. Chem.* 269, 28815–28821.
31. Dierks, E. A., Davis, S. C., and Ortiz de Montellano, P. R. (1998) *Biochemistry* 37, 1839–1847.
32. Manchester, J. I., Dinnocenzo, J. P., Higgins, L., and Jones, J. P. (1997) *J. Am. Chem. Soc.* 119, 5069–5060.
33. Toy, P. H., Newcomb, M., and Hollenberg, P. F. (1998) *J. Am. Chem. Soc.* 120, 7719.
34. Newcomb, M., Le Tadic, M.-H., Putt, D. A., and Hollenberg, P. F. (1995) *J. Am. Chem. Soc.* 117, 3312.
35. Newcomb, M., Le Tadic-Beadatti, M.-H., Chestney, D. L., Roberts, E. S., and Hollenberg, P. F. (1995) *J. Am. Chem. Soc.* 117, 12085.
36. Schroder, D., Shaik, S., and Schwarz, H. (2000) *Acc. Chem. Res.* 33, 139–145.
37. Harris, N., Cohen, S., Filatov, M., Ogliaro, F., and Shaik, S. (2000) *Angew. Chem., Int. Ed. Engl.* 39, 2003–2007.
38. Audergon, C., Iyer, K. R., Jones, J. P., Darbyshire, J. F., and Trager, W. F. (1999) *J. Am. Chem. Soc.* 121, 41–47.
39. Imaoka, S., Yoneda, Y., Matsuda, T., Degawa, M., Fukushima, S., and Funae, Y. (1997) *Biochem. Pharmacol.* 54, 677–683.
40. Li, H., and Poulos, T. L. (1997) *Nat. Struct. Biol.* 4, 140–146.
41. Boddupalli, S. S., Hasemann, C. A., Ravichandran, K. G., Lu, J. Y., Goldsmith, E. J., Deisenhofer, J., and Peterson, J. A. (1992) *Proc. Natl. Acad. Sci. U.S.A.* 89, 5567–5571.
42. Ravichandran, K. G., Boddupalli, S. S., Hasemann, C. A., Peterson, J. A., and Deisenhofer, J. (1993) *Science* 261, 731–736.
43. Yeom, H., Sligar, S. G., Li, H., Poulos, T. L., and Fulco, A. J. (1995) *Biochemistry* 34, 14733–14740.
44. Sevrioukova, I. F., Li, H., Zhang, H., Peterson, J. A., and Poulos, T. L. (1999) *Proc. Natl. Acad. Sci. U.S.A.* 96, 1863–1868.
45. Lu, P., Alterman, M. A., Chaurasia, C. S., Bambal, R. B., and Hanzlik, R. P. (1997) *Arch. Biochem. Biophys.* 337, 1–7.
46. Chang, Y. T., and Loew, G. H. (1999) *Proteins* 34, 403–415.

BI010395E